Entanglement of molecular orientation and vibronic degrees of freedom by ultrafast photoexcitation in an ensemble of initially randomly oriented molecules

Manuel Cardosa-Gutierrez[1], Gaurav Pandey[1], Raphael D. Levine[2,3,4] and Francoise Remacle[1*]

1. Theoretical Physical Chemistry, Research Unit MOLSYS, University of Liege, , 4000 Liège, Belgium
2. Institute of Chemistry, The Hebrew University of Jerusalem, Jerusalem 91904, Israel
3. Department of Molecular and Medical Pharmacology, David Geffen School of Medicine,
4. Department of Chemistry and Biochemistry, University of California, Los Angeles, CA 90095, USA

Abstract

When exciting an ensemble of initially randomly oriented molecules, a linearly polarized few cycle, few fs, UV or NIR pulse entangles the molecular degrees of freedom with the orientations of the molecule during the fast excitation step. We show using fully quantum dynamical studies of an ensemble of initially randomly oriented LiH molecules that the entanglement is not maximal and varies significantly with the pulse parameters. For a few cycle NIR multiphoton excitation, a dozen of dominant orientations suffice to describe the ensemble coherent dynamics while only a few are needed for a one photon UV process. Each principal orientation is correlated with a principal molecular vector made of a superposition of Σ or Π electronic states because of the cylindrical symmetry. For each principal molecular vector, the oscillation of specific electronic coherences drives charge migration and the forces on the nuclei.

* Corresponding author fremacle@uliege.be

TOC

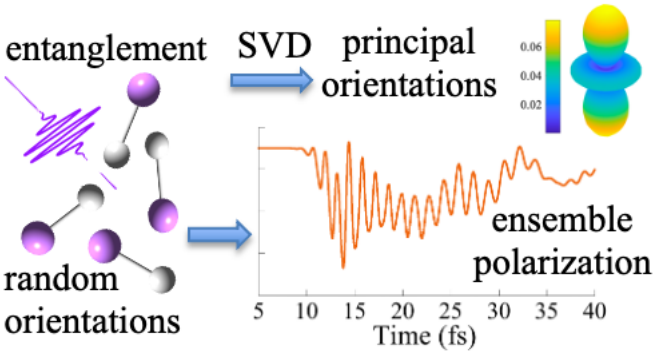
entanglement
SVD
principal
orientations
0.06
0.04
0.02
ensemble
polarization
random
orientations
5
10
15
20
25
30
35
40
Time (fs)

Driving molecular systems with short atto and few fs optical pulses[1, 2] opens the way to excite a superposition of those electronic states that fall within their broad energy bandwidth. The electronic coherences steer the motion of the non-equilibrium electronic density on a purely electronic time scale, before a significant onset of the nuclear motion.[3-7] They induce ultrafast charge migration between different parts of the molecule during which one could implement charge directed reactivity.[8-12] Typically in molecules, bright excited electronic states of different character, e.g., Rydberg, locally excited, are close in energy. As the nuclei begin to move, these states can be non adiabatically coupled among themselves and to dark states, in particular, charge transfer states, already in the Franck Condon (FC) region and its close vicinity. Since electronic states of a different character interact with light differently, the nature of the electronic states taking part in the non equilibrium density can be tuned by adjusting the pulse parameters: carrier frequency, duration, polarization, peak amplitude and the carrier-envelope phase. The ability to control the initial non equilibrium vibronic density therefore opens the way to the design of novel schemes for controlling chemical reactivity, based on entangling selectively the electronic and nuclear degrees of freedom at the excitation step.[13, 14]

We have shown that the pulse parameters can be used to control the fragmentation of diatomic molecules,[15, 16] as well as bond making during the photoisomerization of the medium size norbornadiene molecule. [17] However, for the polarization and the carrier-envelope phase acting as control parameters, one needs to orient the molecules beforehand, [18-22] which cannot be easily implemented for many molecules. [23-25] Even when the molecules can be oriented, there is a distribution of orientations that can prevent for an effective control, the achievable orientation being typically limited to values of $\langle \cos\theta \rangle \approx 0.7$ and $\langle \cos^2\theta \rangle \approx 0.8$.

Here we show that the entanglement between orientations and molecular degrees of freedom is not necessarily maximal and that it can vary significantly according to the multiphoton or one photon character of the excitation. The degree of entanglement is quantified using the Singular Value Decomposition (SVD) approach of the ensemble density matrix into principal orientations that we proposed recently.[26] The Schmidt rank[27] (the number of principal orientations) appears to reflect the one photon or multiphoton character of the excitation which can be controlled by varying the pulse parameters: carrier frequency, duration and peak amplitude. For an ensemble of initially randomly oriented LiH molecules, an essentially one photon excitation by a UV pulse leads to low Schmidt rank of four, the fourth singular

value accounting for the small amount of two photon transitions. On the other hand a NIR multiphoton process leads to larger Schmidt rank values, that can reach a dozen or so for the pulse parameters investigated in this study. As we discuss in detail below, each principal orientation corresponds to a principal molecular vector that is a superposition of several electronic states and therefore exhibits specific electronic coherences. By adjusting the pulse parameters (carrier frequency, peak amplitude, and duration), one can control the number of principal orientations and from which electronic states the principal molecular vectors are combined.

We conclude that control based on electronic coherences is therefore not limited to initially oriented molecules. We show that ensembles of randomly oriented molecules exhibit rich, specific coherent vibronic dynamics in each principal orientation, thereby providing control of the stereodynamics of the ensemble. We illustrate how each principal molecular vector corresponds to specific force on the nuclei that selectively drive nuclear motions and that can be probed by a specific emission dipole.

The time-dependent Schrödinger equation (TDSE) is integrated on a grid of $N_b = N_e \times N_g$ molecular basis functions made of products, $|b>=|g>|e>$, of N_g molecular geometries and N_e adiabatic electronic states.[26, 28] N_o random orientations, $|o>$, of the electric field of the pulse with respect to a fixed orientation of the molecule in the laboratory frame are discretized over the unit sphere. The N_o normalized vectors, $\boldsymbol{c}_o(t)$, of N_b dimensions, corresponding to each orientation, are computed by solving the TDSE, $i\hbar\, d\boldsymbol{c}_o(t)/dt = \boldsymbol{H}(t)\boldsymbol{c}_o(t)$ where $\boldsymbol{H}$ is the full Hamiltonian matrix including the non-adiabatic coupling (NAC) terms and the interaction with the exciting pulse:

$$\boldsymbol{H}(t) = -\frac{1}{2m}(\boldsymbol{\nabla}_R^2 + 2\boldsymbol{\tau}\cdot\boldsymbol{\nabla}_R + (\nabla_R\boldsymbol{\tau}) + \boldsymbol{\tau}\cdot\boldsymbol{\tau}) + \boldsymbol{V}_{pot} - \boldsymbol{E}(t)\cdot\boldsymbol{\mu} \qquad (1)$$

$\boldsymbol{H}(t)$ in Eq. (1) is written for a diatomic molecule in atomic units. m is the reduced mass, $\boldsymbol{\tau}$ is the matrix of the Non Adiabatic derivative Coupling (NAC) between electronic states i and j at grid point g, $\boldsymbol{\tau_{ij}}(g) =< \Psi_i(g)|\boldsymbol{\nabla}_R|\Psi_j(g) >$.[29] In the third term of the kinetic energy operator, $(\nabla_R\boldsymbol{\tau})$, the operator ∇_R is multiplied by the identity matrix, **1**, on left hand side, where R is the internuclear distance. $\boldsymbol{V}_{pot}$ is the matrix of the potentials of the electronic states. The interaction between the electric field of the polarized short pulse, $\boldsymbol{E}(t)$, and the charge density of the molecule entangles orientations and vibronic molecular degrees of freedom. It is included in the dipole approximation, $-\boldsymbol{E}(t)\cdot\boldsymbol{\mu}$. $\boldsymbol{\mu}$ is the matrix of the electric dipole, $\boldsymbol{\mu} = \boldsymbol{\mu}_{nucl} + \boldsymbol{\mu}_{el}$. The time profile of the electrical field is given by $\boldsymbol{E}(t) = -d\boldsymbol{A}(t)/dt$. $\boldsymbol{A}(t) = -\hat{\boldsymbol{e}}\left(E_0/\omega_p\right)f(t)\sin\left(\omega_p\left(t-t_p\right)+\phi\right)$ where $\hat{\boldsymbol{e}}$ is the polarization

direction of the pulse, E_0 its peak amplitude, ϕ the carrier envelope phase and ω_p its carrier frequency. $f(t)$ is a Gaussian envelope of Full Width at Half Maximum (FWHM), $2\sqrt{2\ln 2}\,\sigma_p$, centered at t_p.

The coherent wave function, $|\Psi_{ens}(t)>$, is a $N_b \times N_o$ vector, made by stacking the N_o $\boldsymbol{c}_o(t)$ vectors:

$$|\Psi_{ens}(t)>=(1/\sqrt{N_o})\sum_o^{N_o}\sum_b^{N_b} c_{bo}(t)|b>|o> \quad (2)$$

The full density matrix of the ensemble, $\rho_{ens}(t)$, is a pure state density matrix of dimensions $N_b\,N_o \times N_b\,N_o$, $\rho_{ens}(t) = |\Psi_{ens}(t)><\Psi_{ens}(t)|$:

$$\boldsymbol{\rho}_{ens} = \sum_{b,b\prime}^{N_b}\sum_{o,o\prime}^{N_o} c_{bo}(t)c^*_{b\prime o\prime}(t)|b>|o><o'|<b'|, \quad (3)$$

To perform the SVD analysis, $|\Psi_{ens}(t)>$ is matricized into an $N_b \times N_o$ rectangular matrix **B**.[26] Each of the N_o columns of the matrix **B** is a vector $\boldsymbol{c}_o(t)$ (of N_b components) that corresponds to a specific orientation *o,* with typically $N_o \ll N_b$. The principal orientations of the ensemble are determined by SVD of the matrix **B**:

$$\mathbf{B} = \mathbf{U\Sigma V}^{\dagger}=\sum_{v=1}^{N_o}\sigma_v\,\mathbf{U}_v \otimes \boldsymbol{V}_v = \sum_{v=1}^{N_o}\sigma_v\,\mathbf{B}_v \quad (4)$$

The matrix **B** has maximum N_o non zero singular values for $N_o \ll N_b$. Eq. (4) is an exact representation of **B** as a sum of N_o principal separable components. In each principal component *v*, the orientation and molecular degrees of freedom are separable. The left singular vectors, $\mathbf{U}_v$, are the molecular singular vectors, with components on the N_b vibronic basis functions only and the right singular vectors, $\mathbf{V}_\mathrm{v}$, are the principal orientations vectors and have components only on the N_o sampled orientations. The singular values are real and both the $\mathbf{U}_v$ and the $\mathbf{V}_\mathrm{v}$ vectors have complex amplitudes on the vibronic and orientation basis respectively.

Using the SVD of **B** given by Eq. (4), $\rho_{ens}(t)$ can be exactly written as

$$\boldsymbol{\rho}_{ens} = \sum_v^{N_o}\sum_{v\prime}^{N_o}\sigma_v(t)\sigma_{v\prime}(t)|u_v(t)>|v_v(t)><v_{v\prime}(t)|<u_{v\prime}(t)| \quad (5)$$

The molecular, $N_b \cdot N_b$, $\boldsymbol{\rho}^{mol}$, and orientation, $N_o \cdot N_o$, $\boldsymbol{\rho}^{or}$, reduced density matrices are mixtures, given by

$$\boldsymbol{\rho}^{mol} = \mathrm{Tr}_{or}[\boldsymbol{\rho}_{ens}] = \mathbf{B}\mathbf{B}^{\dagger} \quad (6)$$

And

$$\boldsymbol{\rho}^{or} = \mathrm{Tr}_{mol}[\boldsymbol{\rho}_{ens}] = \mathbf{B}^{\dagger}\mathbf{B} \quad (7)$$

with

$$\mathrm{Tr}[\rho^{mol}]=\mathrm{Tr}[\rho^{or}]=\sum_{v=1}^{N_o}\sigma_v^2 = \sum_{v=1}^{N_o} s_v\,,\ \ s_v = \sigma_v^2 \quad (8)$$

Eq. (4) provides an exact description of the matrix **B** when all the N_o nonzero singular values, σ_v, are retained. The maximum Schmidt rank, that is, the number of separable terms necessary to describe $|\Psi_{ens}(t)>$, is N_o, the number of nonzero singular values of the matrix **B**. Typically, as we show in detail below, only a few principal components, N_{min}, are needed to recover the traces of $\boldsymbol{\rho}_{ens}$ and of $\boldsymbol{\rho}^{mol}$ and $\boldsymbol{\rho}^{or}$ to a specified numerical accuracy threshold, thereby leading to an effective lower Schmidt rank of the ensemble density matrix, and providing a significant compaction of the matrix **B**. Furthermore, when there is no additional source of entanglement between the molecular and orientation degrees of freedom after the interaction with the pulse, the left singular vectors of the matrix **B,** $\mathbf{V}_v$, are stationary. The dynamics of the N_{min} $\mathbf{U}_v$ molecular vectors can be computed using the TDSE with the molecular Hamiltonian, $\boldsymbol{H} = -\frac{1}{2m}(\boldsymbol{\nabla}_R^2 + 2\boldsymbol{\tau}\cdot\boldsymbol{\nabla}_R + (\nabla_R\boldsymbol{\tau}) + \boldsymbol{\tau}\cdot\boldsymbol{\tau}) + \boldsymbol{V}_{pot}$, which leads to major saving of computer resources in terms of memory and time.[26]

By construction, SVD provides a set of principal orientation vectors, the $\mathbf{V}_v$ vectors, that are orthogonal to one another. To get insights, we decompose them below on a basis of spherical harmonics, $Y_{lm}(\theta,\varphi)$:

$$V_v = \sum_{l,m} a_{l,m} Y_{lm}(\theta,\varphi) \qquad (9)$$

We computed the dynamics for N_o = 800 initial random molecular orientations up to a time, t_f, after the end of the pulse using the full Hamiltonian (Eq. (1)). The initial state is the ground vibrational wave function of the ground electronic state (GS). The LiH molecule is oriented along the Z axis of the Cartesian frame.The electronic structure parameters (potentials, permanent and transition dipoles, and NAC vectors) are those reported in ref. [30]. The parameters of the NIR pulse are ω_p = 1.54 eV, σ_p = 1.64 fs, FWHM= 3.63fs, $\phi = 0$, corresponding to an energy bandwidth = 1.13 eV, centred at t_p = 12.5 fs. E_0= 0.02 a.u. (1.4 $\times 10^{13}$ W/cm^2). The matrix $\boldsymbol{B}(t_f)$, t_f = 18.6 fs, is constructed and its SVD (Eq.(4)) determines the N_{min} principal molecular vectors, $\mathbf{U}_v$, that are needed to compute the ensemble dynamics after the pulse. The multiphoton processes induce a rich ensemble transient dynamics during the pulse, particularly among the excited Σ states that are strongly coupled by the NAC in and at the exit of the FC region, Figures 1a and 1c. Σ_1 is populated by a two photon process and acts as a doorway for reaching higher Σ and Π states. Σ_2, Σ_3 , Σ_4 and Σ_5 are populated with one or two additional photons, Π_1 with an extra photon and Π_2 with an extra two photons. For the photon energy, field strength and duration of the NIR pulse used here, Π_1 cannot be reached by a two-photon transition from the ground state.

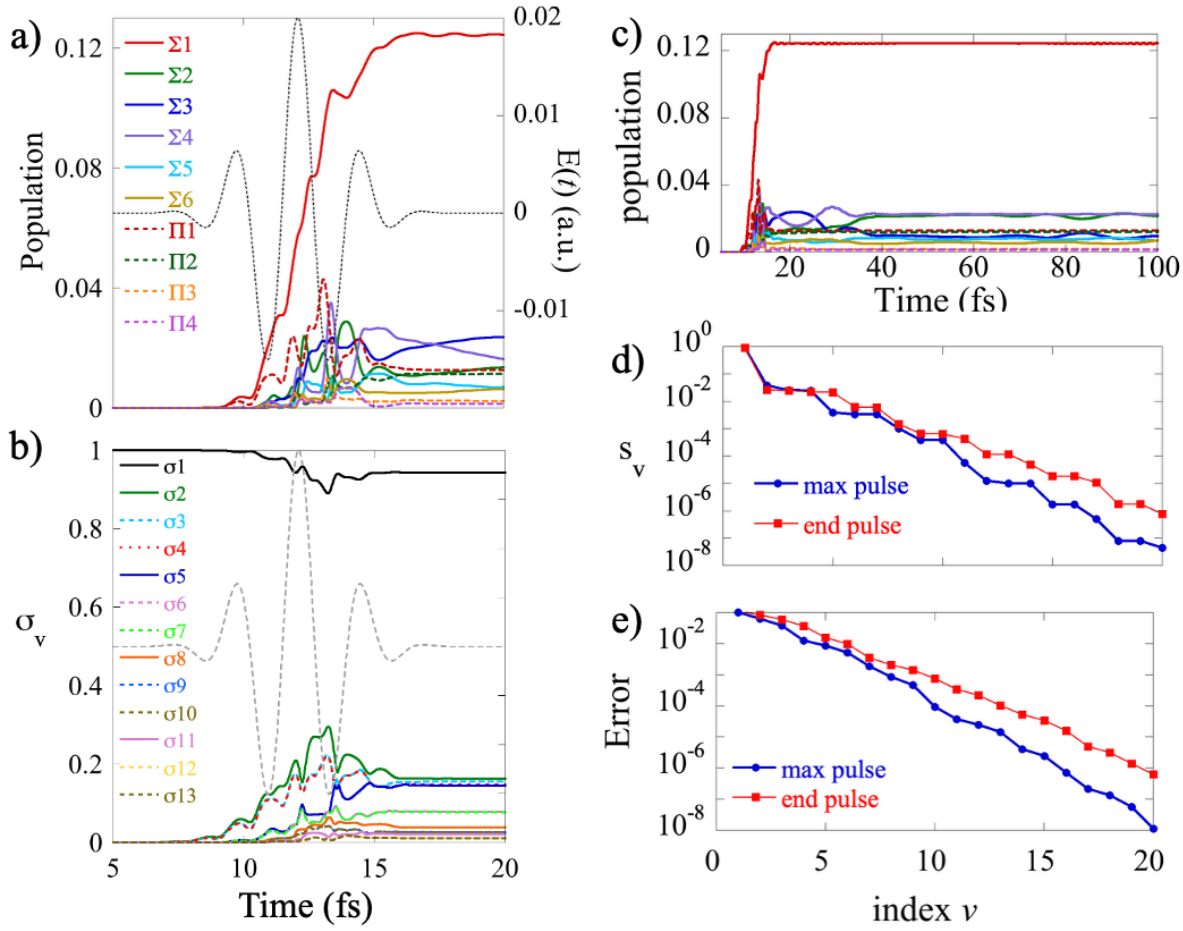

Figure 1 : Population dynamics computed for an ensemble of initially randomly oriented LiH molecules during the pulse (a), and at longer time (c). b) The time evolution of the singular values during the pulse. Singular values with principal orientations on X and Y of the Cartesian frame, see figure 2 below, are degenerate, and plotted in dashed lines, the time profile of $E(t)$ (right ordinate) is shown in black dashed lines. d) Squared singular values, s_v and e) Error on the norm of the molecular density matrix as a function of the index v at the maximum of the pulse, t_p , and at the end of the pulse, t_f, on a log scale, see SI Figures S5 to S8 for results for NIR pulses of different peak amplitude and duration.

The values of the largest 13 singular values, σ_v , during the pulse are reported in Fig. 1b as a function of time. They oscillate significantly, reflecting the transient population dynamics, and become stationnary when the pulse is over. They decrease sharply with the v index as can be seen from Figure 1d where their square values, s_v, are plotted at the maximum and at the end of the pulse as a function of the v index on a log scale. The corresponding error on

$\mathrm{Tr}[\rho^{mol}]$, $\Delta[\rho_v] = 1 - \sum_{i=1}^{v} s_i$, is reported in Figure 1e. N_{min}=13 singular components are needed for reaching an numerical accuracy of 10^{-4} on the norm of ρ^{mol}, providing a measure of the effective entanglement between the orientation and molecular degrees of freedom induced by the NIR multiphoton excitation. By contrast, only four σ_v are needed to reach the same accuracy level on the $\mathrm{Tr}[\rho^{mol}]$ for the essentially one photon excitation by a few cycle, 2fs FWHM, 5.17 eV UV pulse with E_0 = 0.01 a.u.. This pulse promotes only a few percent of population to the excited Σ and Π states, see ref. [26] and SI, section S1, Figure S1 for more details. A lower peak amplitude of the NIR pulse of E_0 = 0.01 a.u. reduces the amount of three and more photon absorption and therefore the number of principal orientations needed to keep an accuracy of $\Delta[\rho_v] = 10^{-4}$ is N_{min}=8. Using the same lower peak amplitude and doubling the duration of the pulse (7.26 fs) requires N_{min}=7. For the 7.26 fs pulse duration, the amount of two photon transition to Σ_1 increases leading to a higher population in Σ_1, but not to higher populations in higher excited states because the narrower bandwidth does not allow to meet resonance conditions. These results are dicussed in the SI, section S2, Figures S5 to S8.

The N_{min}=13 principal orientations correspond to the increasing orders of the multiphoton processes that are allowed by optical selection rules for an electronic density of cylindrical symmetry averaged over initially random orientations. The principal orientations, $\boldsymbol{V}_v$, correspond to principal molecular vectors, $\mathbf{U}_v$, localized either in the Σ or Π manifold, with projections of the orbital angular momentum, Λ, on the molecular axis, $\Lambda = 0$ for Σ states and $\Lambda = \pm 1$ for the Π. When decomposed on spherical harmonics with Eq. (9), a principal orientation vector $\boldsymbol{V}_v$, corresponding to a molecular $\mathbf{U}_v$ vector localized on Σ states has therefore weights on $Y_{l,0}(\theta, \varphi)$ (m =0) harmonics only while a principal orientation corresponding to a molecular vector $\boldsymbol{U}_v$ localized on Π states has weights on $Y_{l,\pm 1}(\theta, \varphi)$ ($m = \pm 1$). The values of l reflect the order of the multiphoton processes contributing to each principal orientation.

We show in Figure 2 the localization of the $\mathbf{U}_v$ vectors on the electronic states along the internuclear distance R and heatmaps of localization of the $\mathbf{V}_v$ vectors. The coefficients of the $\mathbf{V}_v$ vectors on spherical harmonics, Eq. (9), are reported in Table S1. The largest singular value, s_1, corresponds to a molecular vector $\mathbf{U}_1$ mainly localized on the GS with a small weight on Σ_1 that can be reached by a two-photon excitation, see Figure 2a. The orientation vector, $\mathbf{V}_1$, is essentially uniform with a 0.92 weight on $Y_{0,0}$ and 0.08 weight on $Y_{2,0}$. There are then four components with very similar s_v values, as can be seen from Figure 1d. $\mathbf{U}_2$,

Figure 2b, is localized on Σ_1 with a small weight on the GS and even smaller weights on all the excited Σ states that can be reached by multiphoton excitation. $\mathbf{V}_2$ is oriented along Z with a dominant 0.78 weight on $Y_{2,0}$, and smaller weights on other harmonics (0.08 on $Y_{0,0}$ and on $Y_{4,0}$, 0.05 on $Y_{1,0}$, 0.03 on $Y_{3,0}$ etc... .) The high weight on $Y_{2,0}$ reflects that Σ_1 acts as a bottleneck for reaching the higher excited Σ states. The next singular component corresponds to a $\mathbf{U}_3$ molecular vector localized on excited Σ states above Σ_1, mainly Σ_4, Σ_2 and Σ_3, that can be reached by the absorption of an extra photon from Σ_1, Figure 2c. Accordingly, $\mathbf{V}_3$ is oriented along Z with the highest weights on the odd harmonics on $Y_{1,0}$ (0.63), on $Y_{3,0}$ (0.28) and smaller weights on $Y_{2,0}$ (0.05) and on $Y_{4,0}$(0.02), see Figure 2c. s_4 and s_5 are numerically degenerate. $\mathbf{U}_4$ and $\mathbf{U}_5$ are localized on the two components of the Π_1 and Π_2 states that can be reached by one or two extra photons from Σ_1. $\mathbf{V}_4$ and $\mathbf{V}_5$ are oriented along Y and X respectively. They have high weights on the odd harmonics $Y_{1,\pm1}$ (0.33 on each) with smaller weights on $Y_{2,\pm1}$ (0.14 on each), Figure 2d. s_6 and s_7 are also degenerate, with $\boldsymbol{U}_6$ and $\mathbf{U}_7$ localized on the Π_1 and Π_2 states at slightly larger *R* values, with a maximum on Π_1. $\mathbf{V}_6$ and $\mathbf{V}_7$ are oriented along Y and X with the nearly equal weights on $Y_{2,\pm1}$ (0.21 on each), $Y_{1,\pm1}$ (0.19 on each) and $Y_{3,\pm1}$ (0.07 on each) and $Y_{4,\pm1}$ (0.03 on each), see Figure S4. Figure 2e shows the localization of the s_8 component. $\mathbf{U}_8$ is localized on the excited Σ states, with the highest weight on Σ_2, and exhibits an overtone excitation on the GS. The highest weight of $\mathbf{V}_8$ is therefore on $Y_{3,0}$ (0.63) with smaller weights on $Y_{5,0}$ (0.17) and on $Y_{4,0}$ (0.11). In Figure S3 of the SI, we show the localization of the five largest principal orientation and molecular vectors for a UV excitation with a few cycle 5.17 eV pulse. The first principal orientation is uniform as in the case of the NIR excitation, with a $\mathbf{U}_1$ vector fully localized on the GS. The next three singular values correspond to one photon excitation along Z and Y and X respectively. Only the fifth one, for which $s_5 = 2\ 10^{-4}$, shows an overtone excitation of the GS.

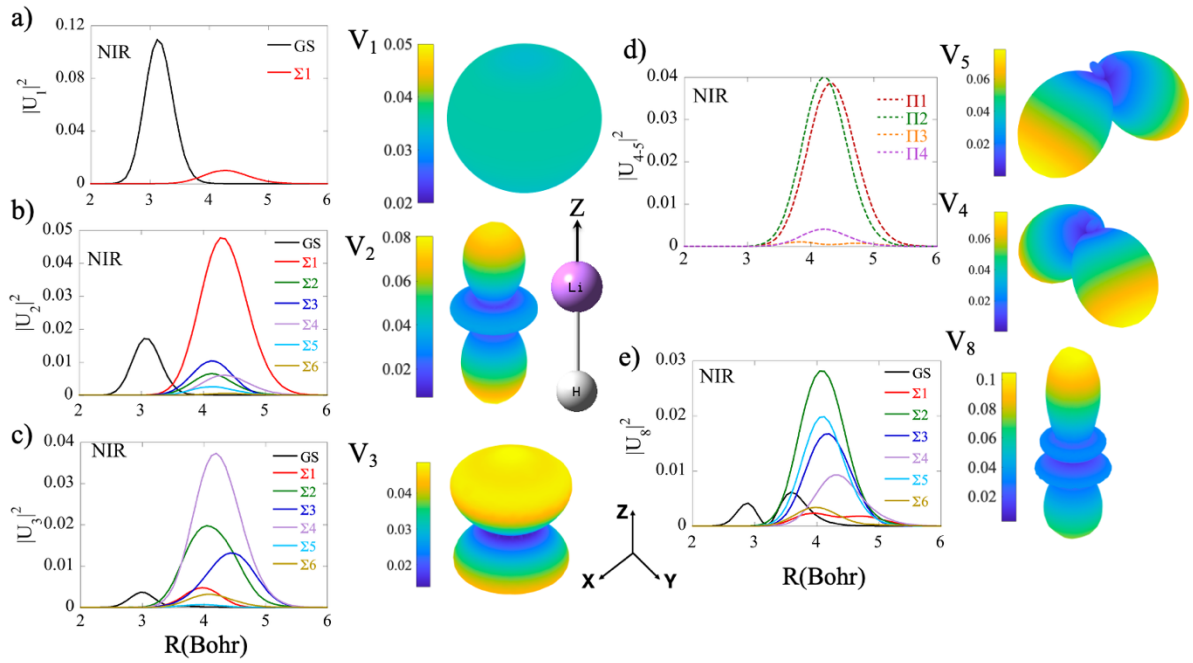

Figure 2. Localization of the $\mathbf{U}_v$ vectors on the molecular basis and heatmaps of the square modulus $\mathbf{V}_v$ vectors, computed after the end of the pulse, at t_f = 18.6 fs. The $\mathbf{V}_v$ vectors v =1 (a), v =2 (b), v = 3(c) and v = 8(e), project on Y_{l0} harmonics and the $\mathbf{U}_v$ vectors localize on Σ states. v = 4, 5 (d) correspond to degenerate principal components with $\mathbf{U}_{v=4,5}$ localized on the two components of the Π states and V_4 and $\boldsymbol{V}_5$ orientated along Y and X with projections on $Y_{l\pm1}$ harmonics. $\mathbf{U}_{v=6,7}$ are also localized on Π states and oriented along Xand Y (See figure S4). The amplitudes of the $\boldsymbol{V}_v$ are given in Table S1 of the SI. See SI, section S2, Figures S5 to S8 for the analysis of of the results for the two weaker NIR pulses.

Figure 2 shows that each molecular vector, $\mathbf{U}_v$, is a vibronic wave packet made of a superposition of specific electronic states, either of Σ or Π symmetry and exhibits specific electronic coherences. Within a principal molecular vector, $\mathbf{U}_v$, there are no electronic coherence between Σ and Π states since the principal molecular vectors are localized either in the Σ or the Π manifold. The electronic states of the molecular principal vectors, $\mathbf{U}_v$, are coupled by NAC during and after the pulse and by the transition dipole which leads to the population transfers seen in Figure 1d.

The ensemble vibronic wave packet exerts a force on the nuclei. The total force is defined using the Ehrenfest theorem, [26]

$$F_{tot} = d\langle \boldsymbol{P}_R \rangle / dt = -\langle \left(\nabla_R \boldsymbol{V_{pot}} \right) \rangle + \langle \left[\boldsymbol{\tau} \ , \boldsymbol{V_{pot}} \right] \rangle + \boldsymbol{E}(t) \, \langle (\nabla_R \boldsymbol{\mu}) \rangle - \boldsymbol{E}(t) \, \langle [\boldsymbol{\tau} \ , \boldsymbol{\mu}] \rangle \quad (10)$$

Where the average is over $|\Psi_{ens}(t) >$ and $\boldsymbol{P}_R = (\hbar/i) \, \boldsymbol{\nabla}_R$ is the momentum operator. The total force, Eq. (10), is made of four terms. The first two terms are governed by the potentials of the electronic states and their couplings [31] The first is the mean value of the potential energy gradients over the electronic states. The second term has no classical analogue and depends on electronic coherences. The next two terms in Eq. (10) are proportional to the time profile of the pulse electric field, **E**(*t*). They are specific for excitation by a short atto or few fs pulse sufficiently broad in energy to access several electronic states and depend on electronic coherences. The dipole terms in the force entangle the molecular degrees of freedom with the orientations. After the pulse is over, only the potential terms contribute to the force and the total force is given by the weighted sum of the specific contributions of each principal molecular vector :

$$\boldsymbol{F}_{tot} = \sum_{v=1}^{N_{min}} s_v \quad \boldsymbol{F_v} \quad (11)$$

Figures 3a shows the total force on the nuclei during the pulse. The dipole terms are of opposite sign and oscillate with half the period of the NIR pulse, their net contribution is slightly negative. The non classical NAC term exhibits fast oscillations that correspond to the periods of the electronic coherence with the GS; they add to the positive potential term that varies monotonically with plateaux when $E(t)$ is close to 0. After the pulse, as the wave packets on the excited states exit the FC region and stop to overlap, the NAC term vanishes. The total force (Figure 3b) is dominated by the potential gradient term of the GS (largest principal component, see Figure 1d) and oscillates with its vibrational period. The recurrence of the wave packet on Σ_1 to the FC region at ≈ 100 fs leads to a revival of the NAC terms of the force. The contribution to the total force of the next three largest principal orientations shown in Figure 2 are plotted in Figure 3 c, d, and e. They contribute each for ≈ 2% to the total force. The *v* =2 component mainly reflects the contribution of Σ_1, which is bound and has a maximum of localization in the range of ≈ 4 Å, see Figure 2b. It is dominated by the potential gradient term. The NAC term is only important when the wave packet on Σ_1 begins to overlap with the GS at the entrance of the FC region. The *v* = 3 term (Figure 3d) is on the other hand dominated by the NAC force and its oscillations reflect the electronic coherences among higher excited Σ states, which are dissociative. The contributions of the *v* = 4 and 5 terms arise from the Π states, only *v* = 4 is shown in Figure 3e. The *v* = 4 term is also dominated by the NAC term and vanishes very early since these states are repulsive. We

show in Figure S3b the total force corresponding to the excitation by the UV pulse. It is over 10 times smaller than the force during the NIR pulse plotted in Figure 3a, while the peak amplitude of the pulse is only 2 times weaker. The reason is the amount of population transferred to excited states is very small. After the UV pulse is over, the total force is fully dominated by the potential gradient term of the GS, without revivals of the NAC term since, for the UV pulse, there is no population in Σ_1, see Figures S1 and S3.

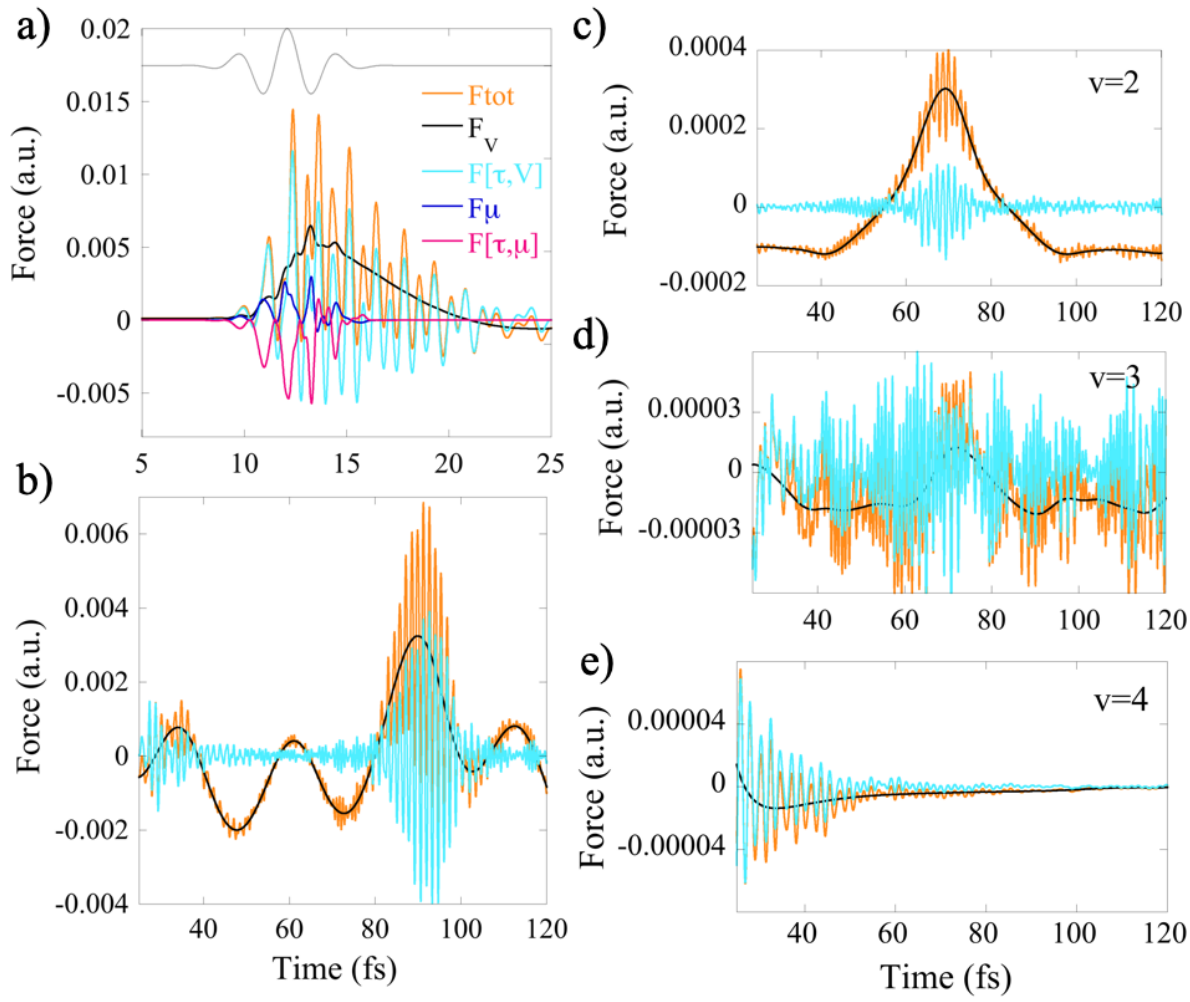

Figure 3. Time profiles of the components of the total force and of $E(t)$ (top) during the pulse (a) and after the pulse (b).c), d) and e) Time profiles of the total force and the potential terms, F_V and $F_{[\tau,V]}$ after the pulse for v = 2, 3 and 4.

After the pulse, the electronic coherences of each principal molecular vector reflect the charge migration between the Li and the H atom. They can be probed by stimulated emission of the total dipole, $\boldsymbol{\mu}_{mol}(t) = Tr[\rho_{mol}(t)\boldsymbol{\mu}]$, which is given by the sum of the dipoles of each of the molecular vectors U_v's :

$$\boldsymbol{\mu}_{mol}(t) = \sum_{v=1}^{N_{min}} s_v \, Tr[\rho_v^{mol}(t)\mu] = \sum_{v=1}^{N_{min}} s_v \, \boldsymbol{\mu}_v(t) \qquad (12)$$

where $\rho_v^{mol}(t)$ is the molecular density matrix of the principal orientation *v*. Since the principal molecular vectors $\boldsymbol{U}_v$ localize either on the Σ or on the Π states, by optical selection rules, the polarizations $\boldsymbol{\mu_v}(t)$ have only a component in the Z direction, along the molecular axis. We show in Figure 4 the time dependence of the polarization after the NIR pulse for the second principal component, $\mu_2(t)$, that is mainly localized on the GS and Σ_1. $\mu_2(t)$ oscillates with the 1.5 fs period of the GS - Σ_1 electronic coherence responsible for the fast charge migration between the Li and H atom. This coherence leads to photon emission either from the Li side or for the H side, as shown by the heatmaps of the dipole emission term $\hat{e} \cdot \mu_2(t)$ plotted in Figure 4a, for random orientations $\hat{e}$ of the probing pulse. In Figure 4b, we show the emission dipole term $\hat{e} \cdot \mu_3(t)$. It oscillates with a longer period of ≈ 8 to 10 fs governed by the electronic coherences between Σ_4 , Σ_3 and Σ_2 of the U_3 molecular vector, which induce a slower charge migration. Figure 4 shows that our approach can be used for disentangling the principal directions of stimulated photo emission and characterizing the electronic coherences of an ensemble of initially randomly oriented electronically and vibrationally excited molecules.

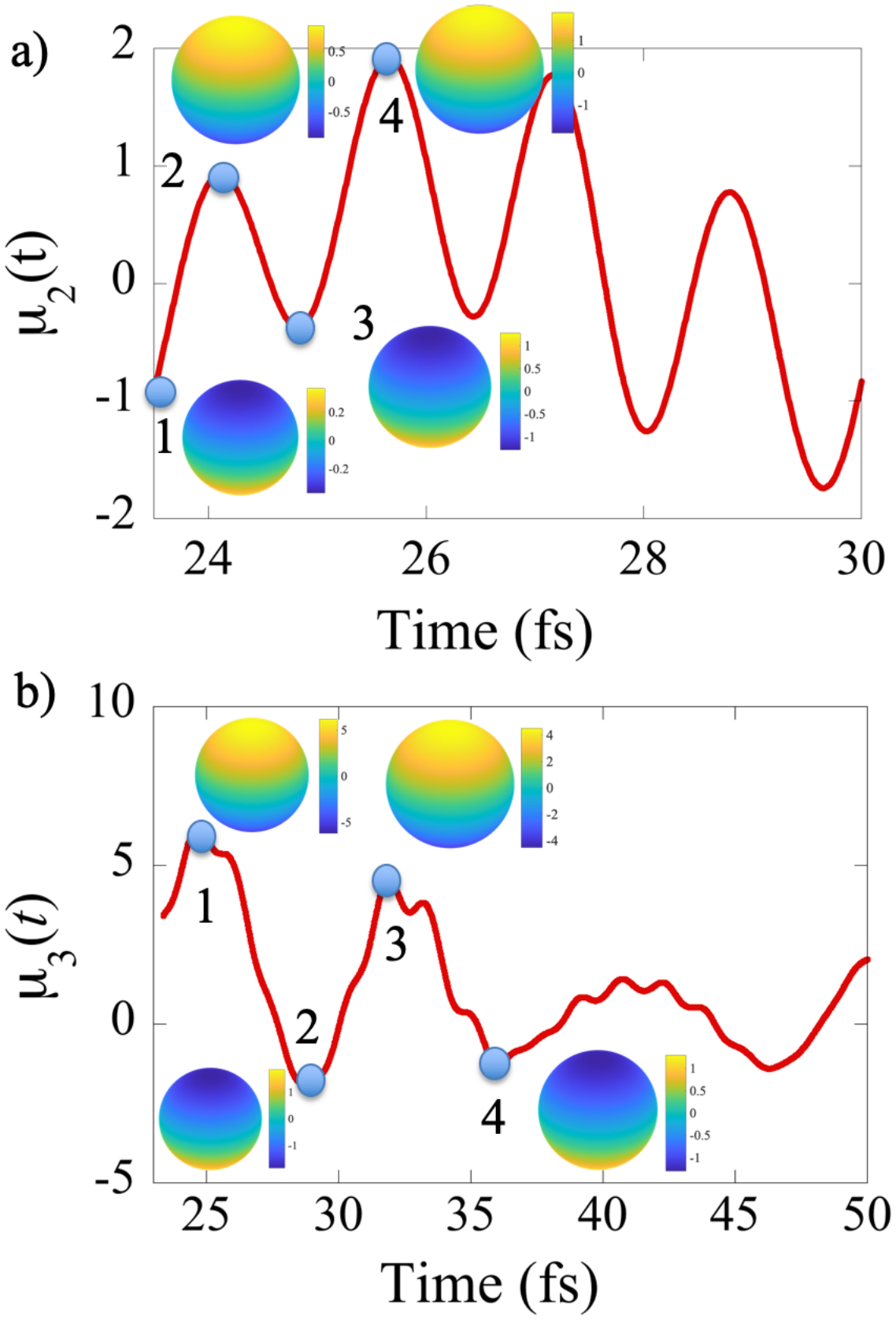

Figure 4 : Emission dipoles $\mu_2(t)$ and $\mu_3(t)$ of the $s_v = 2$ (a) and $s_v = 3$ (b) principal molecular vectors of the ensemble computed for a random orientation of the electric field of

the pulse stimulating the emission. The oscillations of $\mu_2(t)$ emission dipole reflect the fast beatings of charge migration induced by the GS-Σ_1 electronic coherence while those of $\mu_3(t)$ reflects the slower beating induced by the electronic coherences in the $\Sigma_2, \Sigma_3, \Sigma_4$ manifold, which are strongly coupled by NAC. The insets show heatmaps of the emission dipole terms, $\hat{e} \cdot \mu_2(t)$ and $\hat{e} \cdot \mu_3(t)$ at the maxima and minima of the first oscillations, showing emission in the +Z (Li atom) or -Z (H atom) direction.

The engineering of ultra short atto and fs optical pulses opened the way to controlling the dynamics of photoexcited molecules on an ultrafast time scale. An essential quantum feature is exploiting entanglement between electronic and nuclear degrees of freedom built at the excitation step by the broad-in-energy short pulse. Using SVD to analyze the quantum dynamics of an ensemble of initially randomly oriented molecules, we show that few principal orientations suffice to describe the ensemble dynamics, both during and after the pulse. Each principal orientation corresponds to a molecular vector describing a vibronic wave packet delocalized on the nuclear and electronic degrees of freedom, which preserves electronic coherences and electron-nuclear entanglement at the level of the ensemble reduced molecular density matrix. Each molecular component relates to specific features of the quantum force on the nuclei and to specific direction of stimulated emission, which can be used for probing charge migration. The reduced orientation density matrix corresponds to specific orientations which can be decomposed on a basis of spherical harmonics.

We demonstrate that the entanglement by the exciting ultrashort pulse can be selectively engineered in an ensemble of randomly oriented molecules and thereby providing control on the stereodynamics of the ensemble. Our work makes controlling charge migration and chemical reactivity with atto pulses applicable molecular systems that cannot be easily oriented.

Acknowledgments

F.R. , M.C.G and G.P. acknowledge the support of the Fonds National de la Recherche (F.R.S.-FNRS, Belgium), # T.0247.24. Computational resources have been provided by the Consortium des Equipements de Calcul Intensif (CECI), funded by the F.R.S.-FNRS under Grant # 2.5020.11. M.C.G is supported by a fellowship of the Excellence of Science (EOS 40007519) program from the FWO and F.R.S-FNRS.

Supporting Information description: Additional details on the ensemble response to a 2fs UV and to two additional 800nm NIR excitations, additional figures and tables.

References

(1) Krausz, F.; Ivanov, M. Attosecond physics. *Rev. Mod. Phys.* **2009**, *81* (1), 163-234.
(2) Nisoli, M.; Decleva, P.; Calegari, F.; Palacios, A.; Martín, F. Attosecond Electron Dynamics in Molecules. *Chem. Rev.* **2017**, *117* (16), 10760-10825. DOI: 10.1021/acs.chemrev.6b00453.
(3) Remacle, F.; Levine, R. D. An electronic time scale in chemistry. *Proc. Natl. Acad. Sci. USA* **2006**, *103* (18), 6793-6798, 10.1073/pnas.0601855103.
(4) Remacle, F.; Levine, R. D. The time scale for electronic reorganization upon sudden ionization of the water and water-methanol hydrogen bonded dimers and of the weakly bound NO dimer. *J. Chem. Phys.* **2006**, *125* (13), 133321-133327.
(5) Calegari, F.; Ayuso, D.; Trabattoni, A.; Belshaw, L.; De Camillis, S.; Anumula, S.; Frassetto, F.; Poletto, L.; Palacios, A.; Decleva, P.; et al. Ultrafast electron dynamics in phenylalanine initiated by attosecond pulses. *Science* **2014**, *346* (6207), 336-339, 10.1126/science.1254061.
(6) Li, H.; Mignolet, B.; Wachter, G.; Skruszewicz, S.; Zherebtsov, S.; Süßmann, F.; Kessel, A.; Trushin, S. A.; Kling, N. G.; Kübel, M.; et al. Coherent Electronic Wave Packet Motion in C60 Controlled by the Waveform and Polarization of Few-Cycle Laser Fields. *Phys. Rev. Lett.* **2015**, *114* (12), 123004.
(7) Kraus, P. M.; Mignolet, B.; Baykusheva, D.; Rupenyan, A.; Horný, L.; Penka, E. F.; Grassi, G.; Tolstikhin, O. I.; Schneider, J.; Jensen, F.; et al. Measurement and laser control of attosecond charge migration in ionized iodoacetylene. *Science* **2015**, *350* (6262), 790-795. DOI: 10.1126/science.aab2160.
(8) Remacle, F.; Levine, R. D.; Ratner, M. A. Charge Directed Reactivity: a Simple Electronic Model Exhibiting Site Selectivity for the Dissociation of Ions. *Chem. Phys. Lett.* **1998**, *285*, 25-33.
(9) Remacle, F.; Levine, R. D.; Schlag, E. W.; Weinkauf, R. Electronic Control of Site Selective Reactivity: A Model Combining Charge Migration and Dissociation. *J. Phys. Chem. A* **1999**, *103*, 10149-10158.
(10) Cederbaum, L. S.; Zobeley, J. Ultrafast charge migration by electron correlation. *Chem. Phys. Lett.* **1999**, *307* (3–4), 205-210. DOI: http://dx.doi.org/10.1016/S0009-2614(99)00508-4.
(11) Breidbach, J.; Cederbaum, L. S. Migration of holes: Formalism, mechanisms, and illustrative applications. *J. Chem. Phys.* **2003**, *118* (9), 3983-3996.
(12) Kuleff, A. I.; Cederbaum, L. S. Charge migration in different conformers of glycine: The role of nuclear geometry. *Chem. Phys.* **2007**, *338* (2–3), 320-328. DOI: http://dx.doi.org/10.1016/j.chemphys.2007.04.012.
(13) Blavier, M.; Levine, R. D.; Remacle, F. Time evolution of entanglement of electrons and nuclei and partial traces in ultrafast photochemistry. *Phys. Chem. Chem. Phys.* **2022**, *24* (29), 17516-17525, 10.1039/D2CP01440H. DOI: 10.1039/D2CP01440H.
(14) Blavier, M.; Gelfand, N.; Levine, R. D.; Remacle, F. Entanglement of electrons and nuclei: A most compact representation of the molecular wave function. *Chem. Phys. Lett.* **2022**, *804*, 139885. DOI: https://doi.org/10.1016/j.cplett.2022.139885.
(15) Nikodem, A.; Levine, R. D.; Remacle, F. Spatial and temporal control of populations, branching ratios, and electronic coherences in LiH by a single one-cycle infrared pulse. *Phys. Rev. A* **2017**, *95* (5), 053404.
(16) van den Wildenberg, S.; Mignolet, B.; Levine, R. D.; Remacle, F. Temporal and spatially resolved imaging of the correlated nuclear-electronic dynamics and of the ionized

photoelectron in a coherently electronically highly excited vibrating LiH molecule. *J. Chem. Phys.* **2019**, *151* (13), 134310. DOI: 10.1063/1.5116250 (acccessed 2019/10/27).
(17) Valentini, A.; van den Wildenberg, S.; Remacle, F. Selective bond formation triggered by short optical pulses: quantum dynamics of a four-center ring closure. *Phys. Chem. Chem. Phys.* **2020**, *22* (39), 22302-22313, 10.1039/D0CP03435E. DOI: 10.1039/D0CP03435E.
(18) Stapelfeldt, H.; Seideman, T. Colloquium: Aligning molecules with strong laser pulses. *Rev. Mod. Phys.* **2003**, *75* (2), 543-557. DOI: 10.1103/RevModPhys.75.543.
(19) Gordon, R. J.; Zhu, L.; Seideman, T. Coherent Control of Chemical Reactions. *Acc. Chem. Res.* **1999**, *32* (12), 1007-1016. DOI: 10.1021/ar970119l.
(20) Ghafur, O.; Rouzee, A.; Gijsbertsen, A.; Siu, W. K.; Stolte, S.; Vrakking, M. J. J. Impulsive orientation and alignment of quantum-state-selected NO molecules. *Nature Physics* **2009**, *5* (4), 289-293. DOI: Doi 10.1038/Nphys1225.
(21) Kraus, P. M.; Baykusheva, D.; Wörner, H. J. Two-Pulse Field-Free Orientation Reveals Anisotropy of Molecular Shape Resonance. *Phys. Rev. Lett.* **2014**, *113* (2), 023001. DOI: 10.1103/PhysRevLett.113.023001.
(22) Fleischer, S.; Zhou, Y.; Field, R. W.; Nelson, K. A. Molecular Orientation and Alignment by Intense Single-Cycle THz Pulses. *Phys. Rev. Lett.* **2011**, *107* (16), 163603. DOI: 10.1103/PhysRevLett.107.163603.
(23) Zare, R. N. *Angular Momentum, Understanding Spatial Aspects in Chemistry and Physics*; New York; Wiley, 1991.
(24) Bernstein, R. B. *Chemical Dynamics via Molecular Beam and Laser Techniques*; Oxford; Oxford University Press, 1992.
(25) Bernstein, R. B.; Herschbach, D. R.; Levine, R. D. Dynamical aspects of stereochemistry. *J. Phys. Chem.* **1987**, *91* (21), 5365-5377. DOI: 10.1021/j100305a001.
(26) Cardosa-Gutierrez, M.; Levine, R. D.; Remacle, F. Electronic Coherences Excited by an Ultra Short Pulse Are Robust with Respect to Averaging over Randomly Oriented Molecules as Shown by Singular Value Decomposition. *The Journal of Physical Chemistry A* **2024**, *128* (15), 2937-2947. DOI: 10.1021/acs.jpca.3c07856.
(27) Ekert, A.; Knight, P. L. Entangled quantum systems and the Schmidt decomposition. *Am. J. Phys.* **1995**, *63* (5), 415-423. DOI: 10.1119/1.17904 (acccessed 2022/03/24).
(28) Jayantha, S. A.; Komarova, K. G.; Wildenberg, S. v. d.; Remacle, F.; Levine, R. D. AttoPhotoChemistry: Coherent Electronic Dynamics and Nuclear Motion. In *Attosecond Molecular Dynamics*, Vrakking, M. J. J., Lepine, F. Eds.; Vol. 13; Cambridge; Royal Society of Chemistry, 2018; pp 308-347.
(29) Baer, M. *Beyond Born-Oppenheimer: Electronic Nonadiabatic Coupling Terms and Conical Intersections*; Hoboken (NJ); Wiley, 2006.
(30) van den Wildenberg, S.; Mignolet, B.; Levine, R. D.; Remacle, F. Temporal and spatially resolved imaging of the correlated nuclear-electronic dynamics and of the ionized photoelectron in a coherently electronically highly excited vibrating LiH molecule. *J. Chem. Phys.* **2019**, *151* (13), 134310. DOI: 10.1063/1.5116250 (acccessed 2019/10/27).
(31) Smith, F. T. Diabatic and Adiabatic Representations for Atomic Collision Problems. *Phys. Rev.* **1969**, *179* (1), 111-123.